PHYSICAL REVIEW E **81**, 055202(R) (2010)

Steady motion of hairpin-shaped vortex filaments in excitable systems

Sumana Dutta and Oliver Steinbock
Department of Chemistry and Biochemistry, Florida State University, Tallahassee, Florida 32306-4390, USA
(Received 17 December 2009; published 28 May 2010)

We demonstrate the existence of steadily translating filaments in the Belousov-Zhabotinsky reaction. The filaments have self-reinforcing shapes tracing planar hairpins and constant velocities that are inversely proportional to their width. These features are well described by an analytical solution of the mean curvature flow problem. Using numerical simulations based on an excitable reaction-diffusion model, we also probe the solution's large basin of attraction and show that entangled hairpins reconnect during collisions.

DOI: 10.1103/PhysRevE.81.055202 PACS number(s): 05.45.−a, 82.40.Ck, 82.40.Qt

Curvature-dependent motion of curves and surfaces is at the heart of many natural and man-made processes. Such geometric flows are relevant to the evolution of soap films and cell membranes, flame propagation, problems in quantum field theory, as well as applications in image processing [1–3]. The simplest case are planar one-dimensional curves $\mathbf{s}$ that contract according to

$$\frac{d\mathbf{s}}{dt} = \alpha\kappa\hat{\mathbf{N}}, \tag{1}$$

where α describes a system-specific constant line tension, κ equals the local curvature, and $\hat{\mathbf{N}}$ denotes the curve's unit normal vector. Mathematical analyses show that, under this flow, all nonintersecting closed curves evolve toward a circle and vanish in finite time. During the collapse, the enclosed area decreases at a constant rate of $-2\pi\alpha$ [4,5]. Furthermore there are interesting shape-preserving solutions including self-shrinkers such as circles and Abresch-Langer curves, rotating "yin-yang" patterns, and translating curves [2,6].

To date only few of these solutions have been observed in experiments. This situation is surprising because Eq. (1) applies to a wide range of phenomena including two-dimensional grain boundaries and various one-dimensional phase singularities [4]. Among the latter examples, curvature-dependent motion has been used to describe vortex lines in superconductors [7] and scroll wave filaments in excitable and oscillatory reaction-diffusion systems [8].

Scroll waves have been studied in numerous models including the complex Ginzburg-Landau equation (CGLE) [9]. They exist in experimental systems such as the chemical Belousov-Zhabotinsky (BZ) reaction, the cellular slime mold *Dictyostelium discoideum*, and cardiac tissue [10–12]. Especially the latter system attracts considerable attention because scroll waves and their filament dynamics have been linked to dangerous cardiac arrhythmias in humans. Furthermore, negative filament tension induces dynamically interesting chaotic states [12–14].

In general, scroll wave filaments also move in binormal direction at curvature-dependent velocities. This contribution to the overall motion depends in a nontrivial way on reaction kinetics and diffusion coefficients. However, it is zero in the three-dimensional CGLE [9] and also vanishes in excitable systems in which all relevant reaction species have equal diffusion coefficients [15]. Consequently, shape-preserving solutions of Eq. (1) could exist in a broad spectrum of excitable and oscillatory systems. However, this prediction has been tested so far only for circular filament loops [10,16].

In this Rapid Communication, we describe experiments demonstrating the existence of steadily translating filaments in three-dimensional excitable systems. These constant speed constant shape structures are among the hallmark solutions of Eq. (1) and have been referred to as "grim reapers" or hairpins. The study is complemented by numerical simulations based on a FitzHugh-Nagumo-like reaction-diffusion model.

Our experiments employ disk-shaped systems of the ferroin-catalyzed BZ reaction. The disks have a diameter of 10 cm and measure 8.0 mm in height. The lower 4.8 mm of the medium are contained in agrose gel (0.8 % weight/volume) while the upper 3.2 mm are liquid solution. The total height corresponds to approximately 1.7 wavelengths of the excitation vortex. The initial reactant concentrations are constant throughout the two layers: $[H_2SO_4]=0.16$ mol/L, $[NaBrO_3]=0.04$ mol/L, [malonic acid]=0.04 mol/L, and $[Fe(phen)_3SO_4]=0.5$ mmol/L. The corresponding solutions are prepared in nanopure water (18 MΩ cm) and all experiments are carried out at room temperature.

For the creation of scroll waves, we first initiate a nonrotating expanding wave front. This initiation step is carried out by placing a silver wire on the gel-liquid interface for about 20 s, which locally decreases the concentration of inhibitory bromide ions. The shape of the exposed wire controls the shape of the triggered wave and subsequently the form of the filament. Here, we use small localized nuclei creating nearly spherical waves and long wire segments triggering fronts resembling capped cylinders. Then we rapidly swirl the reactant vessel in order to mix the solution phase, which erases the upper portion of the wave. At this time, we also place a glass plate onto the upper solution interface to prevent undesired fluid flow during the main experiment. As the fluid comes to rest, the rim of the gel-bound wave begins to curl spontaneously and nucleates a scroll wave filament of corresponding shape. Notice that the filament loop is formed in very close vicinity of the gel-solution interface and therefore planar.

Detection of wave and filament dynamics is performed by recording image sequences with a charge coupled device (CCD) camera mounted over the system. This method utilizes the color difference between the chemically reduced rest state of the system (red) and its oxidized excitable state

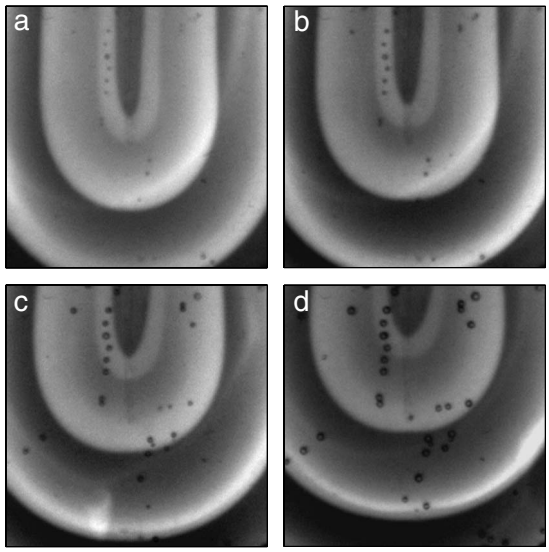

FIG. 1. Four consecutive images of a scroll wave rotating around a hairpin-shaped filament. In (a) the filament extends from the image center upwards. Snapshots are taken at (a) 0.5, (b) 10.5, (c) 31, and (d) 53 min after the initiation of the vortex. Field of view: 1.73×1.73 cm^2.

(blue). In the resulting image data, local gray values are the integrated absorption profiles across the sample height. From these data, we compute the position of the scroll wave filaments by extracting curves that emit waves in alternating fashion in normal and anti-normal direction.

Figure 1 shows a typical sequence of snapshots recorded under the geometric projection described above. The patterns consist qualitatively of bright U-shaped bands which correspond to individual waves of excitation. These bands propagate outwards with the exception of the innermost structure for which the waves move inwards and collide after a short distance [20]. Consequently, the latter band must contain a scroll wave filament which qualitatively matches the shape of the innermost band. The small dark spots in Fig. 1 are slowly growing gas bubbles of the reaction product CO_2.

In separate experiments but for identical conditions, we measure the rotation period of spiral and scroll waves as initially 280 s. The period increases by approximately 20% over a time interval of 2 h and then remains almost constant. These values match the local excitation periods measured for the experiment in Fig. 1 and, hence, confirm the presence of a rotating scroll wave. With respect to this rotation, the frames in Fig. 1 show nearly identical phases. Additional measurements show that, for the given concentrations, filament motion has no detectable binormal component.

The hairpin-shaped filament in Fig. 1 moves slowly toward the upper edge of the image while maintaining a nearly constant width. This motion is in qualitative agreement with the highly curved lower end of the filament and its straight pair of parallel arms. In Fig. 2, two representative examples of such filaments are shown in more detail. The (blue) circles correspond to experimental data and are compared to an analytical solution of Eq. (1) that translates at a constant speed v while maintaining a constant shape of width w.

This solution is found by applying Eq. (1) to the motion

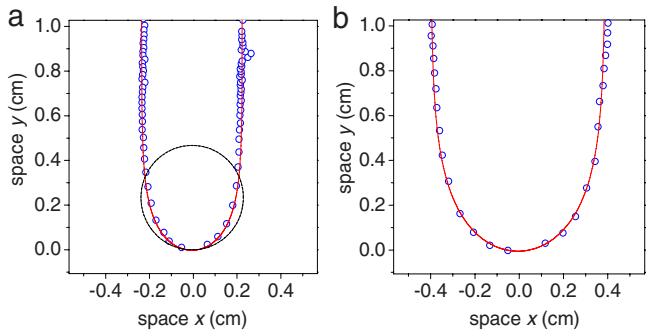

FIG. 2. (Color online) Filament of scroll waves as obtained from two different experiments (open blue circles). The continuous red curves are fits based on the analytical solution in Eq. (2). The dashed (black) curve in (a) shows a circle of diameter w.

of the filament. We reemphasize that the filament is initiated as a planar curve and remains in its plane since motion in binormal direction is negligible. Hence, we analyze the filament dynamics as a two-dimensional problem. For the Cartesian coordinates (x,y), Eq. (1) yields $\partial y/\partial t = \alpha y''/(1+y'^2)$, where the prime denotes partial differentiation with respect to x [2,4]. For translating solutions, $y(x,t) = vt + \tilde{y}(x)$, this differential equation is a Riccati equation of the form $\tilde{y}'' - c\tilde{y}' - c = 0$ with $c = v/\alpha$. It yields

$$\tilde{y}(x) = -\frac{\alpha}{v} \ln \cos\left(\frac{v}{\alpha}(x - x_0)\right) + \tilde{y}_0, \tag{2}$$

where the integration constants x_0 and $\tilde{y}_0$ specify the position of the hairpin turn (in the following set to zero). This solution diverges at $x = \pm \pi\alpha/2v$ and, hence, defines the full width w of the corresponding curve. Consequently, we obtain the simple velocity-width dependence

$$v = \pi\alpha/w. \tag{3}$$

The continuous (red) curves in Fig. 2 are the best least-squares fits of Eq. (2) to the measured filament coordinates. Both fits are in very good agreement with the experimental data. The hairpin widths are $w = 0.47$ cm in (a) and 0.80 cm in (b). For comparison, Fig. 2(a) also shows a circle of diameter w (dotted line), which clearly does not represent the data. Notice that the curvature of the circle is smaller than the hairpin curvature at the origin. Hence, we expect the hairpin to move faster than a circle of identical width. A seemingly related velocity difference had been noted earlier by Keener and Tyson [17] for shrinking noncircular scroll waves which they coined "hot dog" waves. In addition, we note that Panfilov *et al.* [5] used an integral invariant to derive Eq. (3) for similar patterns.

Figure 3 provides quantitative data on the velocity of translating hairpin filaments. Figure 3(a) shows the vertical position y_0 of three filaments of different width as a function of time. The position data are well described by linear functions indicating constant velocities. During the analyzed time intervals, the widths of the hairpins showed no measurable changes (data not shown). We note that the hairpin structures terminate either at the system boundary or with another hairpin that moves in opposite direction. Hence, the structures

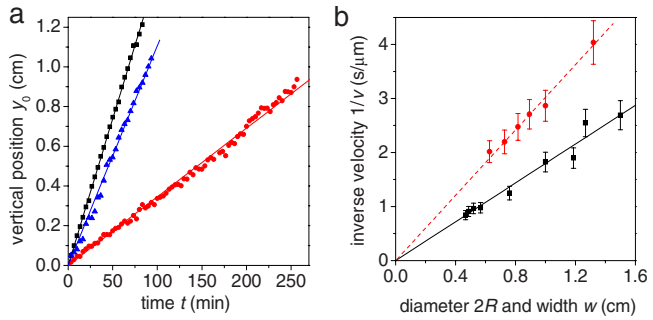

FIG. 3. (Color online) (a) Position of the hairpin turn as a function of time. The three data sets correspond to hairpin widths of $w=0.47$ cm (black squares), 0.57 cm (blue triangles), and 1.27 cm (red circles). (b) Inverse velocity of circular (red circles) and hairpin-shaped (black squares) filaments as a function of diameter and width, respectively. The straight lines are linear fits with zero intercept [see Eq. (3)].

have a finite life time which in the latter case is approximately $t_L=L_0 w/2\pi\alpha$, where L_0 denotes the initial, total "height" of the filament (i.e., the initial distance between the two points of maximal curvature).

The solid (black) squares in Fig. 3(b) represent the inverse velocities of several hairpin-shaped filaments with different full widths w. The measurements are in excellent agreement with the inversely proportional dependence in Eq. (3) and yield a filament tension of $\alpha=(1.77\pm0.05)\times10^{-5}$ cm^2/s. For comparison, we have also measured the initial collapse velocity of circular filament loops. In Fig. 3(b), their inverse values are plotted as a function of the filament diameter $2R$ (solid red circles).

From Eq. (1) and earlier experimental studies [10], we know that circular filaments obey $-dR/dt=\alpha/R$. Hence, the ratio of the two slopes in Fig. 3(b) should equal $\pi/2$. A direct comparison of the experimental data sets in Fig. 3(b) yields a ratio of 1.68 ± 0.1 which differs by only 7% from the expected value. This finding provides additional evidence that the hairpin-shaped filaments are a translating solution of the curvature flow in Eq. (1).

To obtain further insights into these constant-shape solutions, we perform numerical simulation using the Barkley model [18]:

$$\frac{\partial u}{\partial t}=D_u\nabla^2 u+\frac{1}{\epsilon}\left\{u(1-u)\left(u-\frac{v+b}{a}\right)\right\}, \tag{4a}$$

$$\frac{\partial v}{\partial t}=D_v\nabla^2 v+u-v. \tag{4b}$$

In this frequently studied set of reaction-diffusion equations u and v are time-dependent variables. Here, we consider spatially three-dimensional systems with diffusion coefficients $D_u=D_v=1$. The other model parameters are $a=1.1$, $b=0.18$, and $\epsilon=0.02$. The latter values induce excitable point dynamics around a stable steady state. Also notice that for our choice of identical diffusion coefficients (and in the limit of small curvature and twist), filament motion is known to occur strictly in normal direction [19]. Our simulations employ

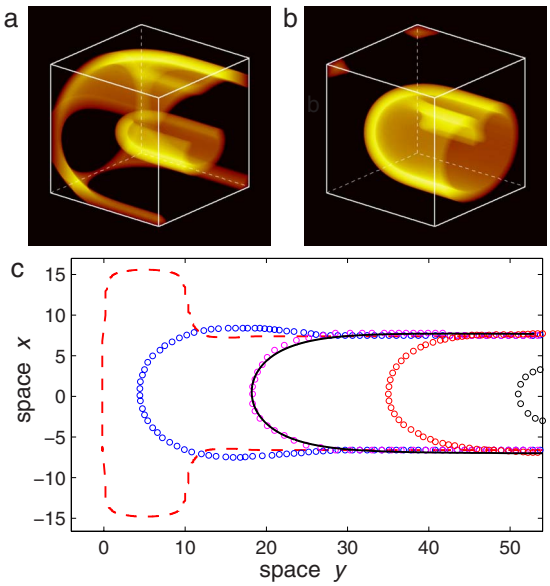

FIG. 4. (Color online) [(a) and (b)] Numerical simulation of a hairpin-shaped scroll wave at opposite phases of one rotation cycle. (c) An initially hammer-shaped planar filament (dashed line) evolves into a stable hairpin which moves rightwards (circles) and agrees well with Eq. (2) (continuous curve).

Euler integration with a time step of 6×10^{-3}. The box-shaped system is surrounded by Neumann boundaries and resolved with $300\times300\times300$ grid points at a grid spacing of 0.2.

We initiate vortex patterns by cutting excitable holes into planar wave pulses. This step nucleates a filament loop of desired shape as the wave edge curls into the void. Figures 4(a) and 4(b) illustrate the v field of such a scroll wave for which the boundary of the "cut-out" region had the shape of the hairpin function in Eq. (2). The two frames show nearly opposite rotation phases. The long-term evolution of the pattern involves the expected translation of the filament [20]. Furthermore, it conserves the width of the hairpin and occurs at (width-dependent) constant speeds.

While all of our observations indicate that the log−cos shape is a stable solution, it is unclear what family of filaments evolve into this structure and at what rate. For this purpose, we have carried out some exploratory simulations in which we varied the initial filament geometry. Figure 4(c) shows an example in which the initial filament describes a planar hammer-shaped curve. Neighboring curves differ by approximately five periods of scroll wave rotation with the leftmost curve being the earliest. Notice that the corners of the filament round off first, followed by the decay of the hammer head feature. Subsequently, the filament rapidly evolves toward the hairpin solution as illustrated by the continuous (black) curve which is obtained by fitting Eq. (2) to one of the simulated filaments. We did not detect any effects caused by the system boundaries. In general, our simulations support the intuitive view that all filament loops (and boundary-bound half loops) of high aspect ratio evolve toward Eq. (2) if large parts of them consist of parallel lines. In addition, the curved part of the hairpin solution and its velocity [Eqs. (2) and (3)] should also be good descriptions if

the hairpin arms are curves of low curvature that maintain a constant or slowly varying distance.

Lastly, we briefly discuss interactions between translating hairpins. In a common plane, two of these filaments can typically not overlap. However, they might form a nested pair if they have different widths. In the latter case, the outer filament propagates at a lower velocity than the inner one, which causes a steadily increasing distance between their turning points. Filament collisions occur only if the hairpins are entangled. To better understand the behavior of such entangled filaments, we performed numerical simulations based on Eqs. (4), in which two perpendicular hairpins of identical width move in antiparallel directions. Already prior to the collision, the turn region of the filaments bend periodically in and out of the main filament plane, while the linear arms show no or little change. Nonetheless, the distance between the hairpin tips decreases and eventually results in a collision. During this collision the hairpins reconnect and form two separate, disentangled filaments. A detailed analysis of the reconnection process will be reported elsewhere. However, the collision outcome reveals a clear difference between the filament hairpins and conventional solitons as the latter emerge from collisions unchanged.

In conclusion, we have demonstrated that scroll wave filaments can have self-reinforcing shapes that travel at constant speed. These shapes and their velocities are well described by classic curvature flow. Accordingly, we expect that vortex filaments in excitable and oscillatory systems should also reveal other characteristic solutions such as rotating non-Archimedean (yin-yang) spirals. Clearly those patterns are closely dependent on the homogeneity and isotropy of the system. Future work will aim to observe these planar solutions experimentally and to identify more complex, stable solutions in three dimensions.

This material is based upon work supported by the National Science Foundation under Grant No. 0910657.

[1] H. T. McMahon and J. L. Gallop, Nature (London) **438**, 590 (2005).
[2] I. Bakas and C. Sourdis, J. High Energy Phys., 2007(06) 057.
[3] R. Malladi and J. A. Sethian, Proc. Natl. Acad. Sci. U.S.A. **92**, 7046 (1995).
[4] W. W. Mullins, J. Appl. Phys. **27**, 900 (1956).
[5] A. V. Panfilov, R. R. Aliev, and A. V. Mushinsky, Physica D **36**, 181 (1989).
[6] U. Abresch and J. Langer, J. Diff. Geom. **23**, 175 (1986).
[7] W. E, Physica D **77**, 383 (1994).
[8] J. P. Keener, Physica D **31**, 269 (1988); B. Echebarria, V. Hakim, and H. Henry, Phys. Rev. Lett. **96**, 098301 (2006).
[9] M. Gabbay, E. Ott, and P. N. Guzdar, Phys. Rev. Lett. **78**, 2012 (1997).
[10] T. Bánsági, Jr. and O. Steinbock, Phys. Rev. Lett. **97**, 198301 (2006).
[11] O. Steinbock, F. Siegert, S. C. Müller, and C. J. Weijer, Proc. Natl. Acad. Sci. U.S.A. **90**, 7332 (1993).
[12] R. H. Clayton, E. A. Zhuchkova, and A. V. Panfilov, Prog. Biophys. Molec. Biol. **90**, 378 (2006).
[13] E. M. Cherry and F. H. Fenton, New J. Phys. **10**, 125016 (2008).
[14] V. N. Biktashev, A. V. Holden, and H. Zhang, Philos. Trans. R. Soc. London, Ser. A **347**, 611 (1994); T. Bánsági, Jr. and O. Steinbock, Phys. Rev. E **76**, 045202(R) (2007).
[15] J. P. Keener and J. J. Tyson, SIAM Rev. **34**, 1 (1992).
[16] M. Vinson, S. Mironov, S. Mulvey, and A. Pertsov, Nature (London) **386**, 477 (1997).
[17] J. P. Keener and J. J. Tyson, Science **239**, 1284 (1988).
[18] D. Barkley, Phys. Rev. Lett. **72**, 164 (1994); D. Margerit and D. Barkley, Chaos **12**, 636 (2002).
[19] S. Alonso, R. Kähler, A. S. Mikhailov, and F. Sagues, Phys. Rev. E **70**, 056201 (2004).
[20] See supplementary material at http://link.aps.org/supplemental/10.1103/PhysRevE.81.055202 for movies of a typical experiment and simulation.